**Batteries & Supercaps**

Research Article
doi.org/10.1002/batt.202300382

Chemistry
Europe
European Chemical
Societies Publishing

www.batteries-supercaps.org

# Improved Vanadium Flow Battery Performance through a Pulsating Electrolyte Flow Regime

Renée De Wolf,[a] Alana Rossen,[a] Michiel De Rop,[a] Luis Fernando Arenas,[a] Tom Breugelmans,[a] and Jonas Hereijgers*[a]

The interest in flow batteries as energy storage devices is growing due to the rising share of intermittent renewable energy sources. In this work, the performance of a vanadium flow battery is improved, without altering the electrochemical cell, by applying a pulsating flow. This novel flow battery flow regime aims to enhance performance by improving its mass transfer properties. Both the pulse volume and frequency have an influence on the battery performance, and lead to a 38.7 % increase in accessible discharge capacity compared to the conventional steady flow regime at values of 0.40 cm$^3$ and 2.4 Hz in this cell, respectively. Furthermore, at these parameter settings a reduction of the mass transfer resistance by 71.4 % is achieved at 0.2 cm$^3$/min·cm$^2$. These results show that a pulsating flow can be beneficial in certain conditions, opening new possibilities for boosting performance in flow batteries.

## Introduction

Renewable energy sources are gaining more interest as an alternative to fossil-based energy sources, yet they are of an intermittent and variable nature. This is a disadvantage, as the power grid requires the ability to provide sufficient electricity at any given moment. Although fossil-based energy production is more flexible, its negative effects on global warming must still prompt a shift towards renewable energy sources such as wind and solar power. As a result, the share of renewable energy in Europe has increased to 22.2 % in 2021 compared to only 10.2 % in 2005.[1] In order to sustain further increase of this share without resulting in an unreliable electrical grid, the incorporation of energy storage is necessary.[2,3] In fact, without available energy storage carbon-based power cannot be eliminated in the short and mid-term.[4]

A promising energy storage technology to prevent grid imbalance is found in flow batteries (FBs). FBs have gained significant attention in recent years due to their possibility in meeting the growing demand for large-scale, sustainable, and low-cost energy storage.[5–9] In comparison to conventional secondary batteries such as lead acid or lithium systems, the electrolyte in a FB is non-static, circulating between storage tanks and electrochemical cells. As a result, the storage capacity is decoupled from the cell size and the capacity can be scaled up independently from the power output.[8–11] Mass transport is critical for obtaining high power output in FBs. Thus, the most common electrodes in FBs are three-dimensional (3D) porous structures in the form of a carbon cloth or graphite felt, which increase the mass transport rate of the electroactive species towards/from the electrode surface, in addition to having a large surface area.[12–17] Regarding efforts towards improving the performance of FBs, important aspects have been considered, such as electrocatalytic activity of electrodes,[18] as well as strategies that do not change the composition of the material, such as electrode compression, flow field configuration, and structural modification of the electrodes.[19]

A first strategy to adjust electrode performance is to vary its compression in the FB. Compression influences cell performance by changing the physical characteristics of the porous material, such as its electrical resistance and contact resistance, and flow properties derived from its permeability.[20] For instance, Ghimire et al. demonstrated that a 25 % compression of the felt electrode results in an optimal FB performance in relation to the trade-off between a reduced electrical resistance and an increased pressure drop.[21] Lu et al. have also shown that capacity loss during cycling, caused by vanadium crossover, can be decreased when the FB is designed in such a way that the positive electrode is compressed by 81 % whereas the negative electrode is compressed by 33 %.[22] However, Charvát et al. reported that the influence of the compression level varies when different felt materials are employed. An optimal compression of 60 % and 30 % was determined for felt electrodes based on rayon and polyacrylonitrile (PAN), respectively, which had a similar porosity and areal weight. This significant difference was attributed to different electrical behaviour and textural properties.[23]

A second strategy is to implement a suitable flow field design to feed the porous electrode with electrolyte in an efficient way. The flow field determines the electrolyte flow pattern in the cell, ideally distributing the electrolyte uniformly within the porous electrode at a high mass transport rate.[24] The utilisation of parallel, serpentine, and interdigitated flow field designs are usually alternatives to the classic flow-by and flow-through configurations in a rectangular channel. Addition-

**Batteries & Supercaps**

Research Article
**doi.org/10.1002/batt.202300382**

**Chemistry Europe**
European Chemical
Societies Publishing

ally, complex shapes such as spiral or circular flow fields, equal path length flow fields and even slotted electrodes have been reported.[20,25–27] While a positive influence on the FB performance was demonstrated by combining porous electrodes with flow fields,[25,28] some designs can result in increased pumping losses, while the introduction of sharp edges can result in faster corrosion of bipolar plates and membrane shearing.[27,29]

Another approach to address the issue of uneven electrolyte distribution and to simultaneously reduce pumping losses, is to incorporate structural modifications directly into the porous electrode. This strategy has already demonstrated promising outcomes. For instance, in our previous work, structured 3D electrodes based on common static mixer designs were indirectly 3D printed and compared to felt electrodes.[30] While the electrochemical performance was similar, the power consumption was reduced by two to three orders of magnitude. Forner-Cuenca et al. also conducted a study comparing different types of traditional carbon-based electrodes, including cloth, paper, and felt.[31] Among them, the cloth demonstrated the lowest pressure drop and highest current density. The woven structure of the cloth provides a regular and periodic shape, resulting in high permeability due to clear electrolyte pathways. Similarly, Tenny et al. investigated various wave patterns in cloth electrodes but faced challenges in determining the most efficient pattern when considering multiple performance metrics. This emphasises the difficulty in identifying an optimal electrode structure.[32]

Finally, an innovative and alternative strategy to increase the mass transfer in FBs is to alter the electrolyte flow regime by adding pulsations to a steady net flow rate. This has been demonstrated for multiple chemical technologies. For instance, Ni et al. compared the mass transfer of oxygen into yeast culture and re-suspension in a stirred tank fermenter and a batch pulsed baffled bioreactor.[33] The results showed that the volumetric mass transfer coefficient increased by 75% on average in the pulsed reactor. Furthermore, Reis et al. developed a micro-bioreactor to produce ɣ-decalactone in which an oscillatory flow regime was employed. Intensive mixing at laminar flow conditions was achieved, leading to a 50% reduction of the time required to obtain the maximum concentration of the product.[34] Hence, pulsating flow has gained interest with electrochemists due to the proved positive influence on the mass transfer in reactors in general. For instance, Pérez-Gallent et al. showed that the single pass conversion in an electrolyser can be doubled by implementing a pulsating flow, while selectivity improvements of 15–20% can be achieved.[35] The increase of conversion can be explained by the fact that the mass transfer increased without influencing the mean residence time, as this remains controlled by the net flow rate applied to the reactor.[36–39] Additionally, in previous work of our group the combination of pulsating flow and pillar field electrodes was investigated, utilising the ferri-ferrocyanide redox couple.[40] This work revealed a fourfold increase in the average limiting current density compared to operation under a conventional steady-state flow regime. Gomaa and Taweel also concluded that combining turbulence promoters with a pulsed flow regime can lead to a 77-fold increase in the mass transfer

rate at the solid-fluid interface.[41] Yet another example is by Yahya et al., who studied the effect of a cathode pulsating flow on the mass transport and performance of a solid oxide fuel cell.[42] Their results showed that the power output increased by an enhanced oxygen diffusion, improving the convective species transport to the reaction sites.

To the best of our knowledge, the only attempt to investigate some type of pulsating flow in a FB was performed by Ling et al., during which they alternated a steady flow rate with static periods.[43] Their findings suggest that utilising a short flow period followed by a long flow termination period, in the order of 5 to 20 s, leads to enhanced energy efficiencies up to 80.5%. Moreover, this approach achieved a significant 50% reduction in pumping costs.[43] However, while these results demonstrated the potential for optimising operational parameters to enhance energy efficiency and cost-effectiveness, no pulsating flow regime in the traditional sense, with a back-and-forth motion while keeping a constant net flow rate, was employed, being instead an intermittent pump operation. As a result, the generation of eddies or vortices by merely turning the pump on and off is highly unlikely as this requires a reversing flow around sharp edges to release the boundary layer from the object.[44] A full pulsating flow regime leads to improved circumstances for eddies to form, breaking the diffusion layer at the surface and improving the mass transfer.

In this work we studied for the first time the influence of adding pulsations to the electrolyte flow of an all-vanadium FB (VFB), showing both the effect of the pulse volume (PV) and the pulse frequency (PF) on the FB performance in comparison to the conventional steady flow regime and in contrast to the intermittent flow regime. As a result of the reciprocating motion of the pulsators, PV corresponds here to half of a peak-to-peak amplitude of the motion. The VFB was chosen from a large variety of FB chemistries because it is the most commercialised and studied chemistry. The active species in both electrolytes are the same which eliminates irreversible capacity loss due to ion crossover through the ion exchange membrane. The electrolytes can be mixed to reverse the crossover, leading to an extended lifespan.[10,45] Additionally, VFBs are inherently stable without risk of thermal runaway or fire under short circuit.[10,46] Therefore, the VFB is a suitable candidate for application in large scale energy storage systems. However, pulsating flow is essentially chemistry agnostic and can also be applied to other types of FBs. The implementation of new mass transfer enhancement strategies could indicate pathways for more efficient devices. By improving the performance of FBs, these technologies could better contribute to the development of sustainable human activity.

## Results and Discussion

### Capacity behaviour during discharge

In order to compare the effect of mass transfer enhancement on the VFB operating at different flow rates, voltage vs capacity curves were recorded. When pulsations were absent (Figure 1A)
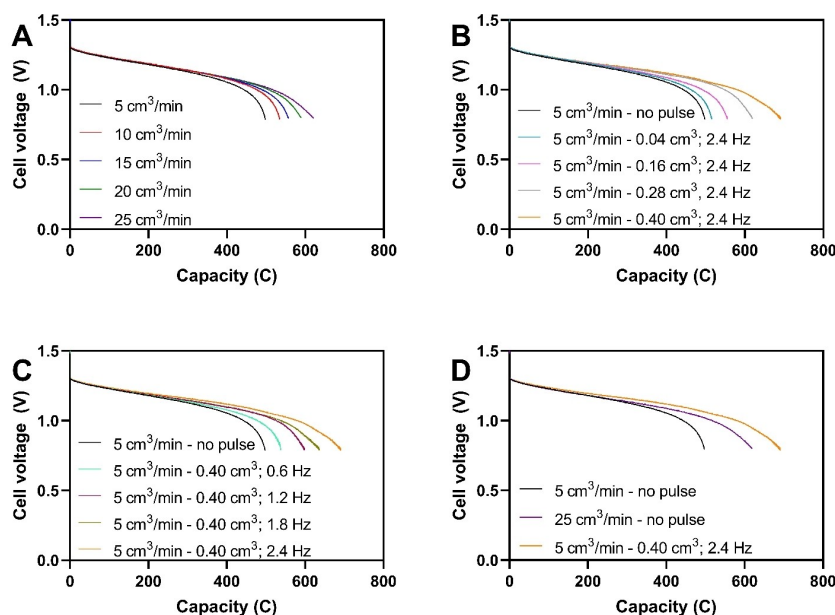
**Figure 1.** A) Cell voltage vs. discharge capacity curves at a constant current of 100 mA/cm² for various flow rates without pulsations; B) various PF settings at a constant flow rate of 5 cm³/min and PV of 0.40 cm³/min; C) various PV settings at a constant flow rate of 5 cm³/min and a PF of 2.4 Hz; and D) at flow rates of 5 cm³/min and 25 cm³/min without pulse compared to 5 cm³/min with pulsations of 0.40 cm³ PV and 2.4 Hz PF.

an increasing flow rate of the electrolyte resulted in a greater accessible capacity during discharge, rising from 498.3 C at 5 cm³/min to 621.0 C at 25 cm³/min. Under a galvanostatic regime, this effect was expected as it is a consequence of the enhanced mass transfer decreasing electrode overpotentials, delaying the onset for the cell voltage cut-off values and thus extending the accessible capacity (and time of discharge before the cut-off). However, the results show that the increase in accessible capacity is not directly proportional to the flow rate. While the mass transfer rate was improved at a higher flow rate, the single-pass reactant conversion is decreased due to the shorter residence time. Aaron et al. came to the same conclusion by determining the limiting current density of a VFB at flow rates between 0.5 cm³/min and 25 cm³/min in a 5 cm² electrochemical flow cell with an area specific resistance (ASR) of 0.6 Ω·cm²;[54] their limiting current density augmented over that range by a factor of 7.8 whereas the singe-pass conversion dropped from 25.2% to 4.0%.

As to the influence of introducing pulsations to the electrolyte flow of the VFB, the PF and the PV were first considered independently. To study the influence of the PF, a constant PV of 0.40 cm³ was chosen. Meanwhile, to investigate the influence of PV a constant PF of 2.4 Hz was selected. In both cases a constant net flow rate of 5 cm³/min was employed. The results are shown in Figure 1(B and C) and reveal that the battery discharge accessible capacity improved each time that a pulsating parameter was risen. Numerical values are given in the Supporting Information (Table S1). When examining the combinations of different PVs and PFs (Figure 2), it became clear that increasing the PV and PF up to 0.07 cm³ and 0.4 Hz, respectively, did not lead to an improved capacity utilisation. After surpassing these thresholds, an enhancement of accessible capacity was possible. Generally, when both pulsation
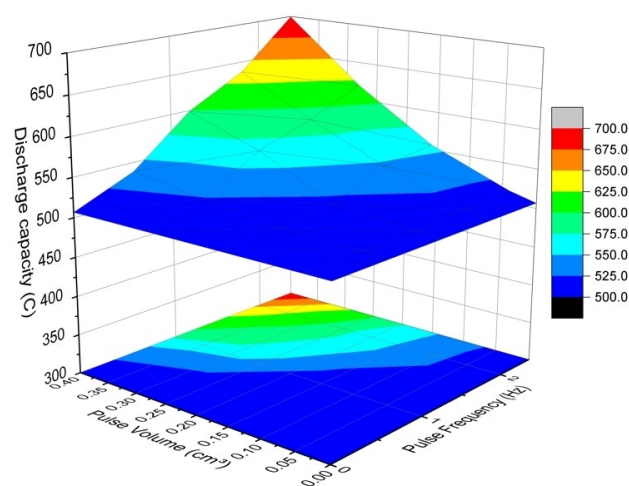


**Figure 2.** Discharge capacities at a constant current of 100 mA/cm² and a constant net flow rate of 5 cm³/min as a function of PV and PF.

parameters were increased the performance improved. At the maximum settings, PV 0.40 cm³ and PF 2.4 Hz, the discharge capacity improved by a significant 38.7% compared to the same net flow rate without pulsations. Since the same net flow rate is employed, it can be established again that the single pass conversion increased. Furthermore, this 38.7% increase in discharge capacity surpassed the performance achieved at a constant steady-state flow of 25 cm³/min (Figure 1D). Therefore, a fivefold reduction of the net flow rate is possible in these conditions without performance losses by applying a pulsating flow regime.

Regarding the battery capacity utilisation, the present VFB afforded up to 5.97% (691.0 C) of its theoretical value at 5 cm³/min with pulsations of 0.40 cm³ PV and 2.4 Hz PF (Figure 1D).

This is explained by the relative low net flow rate of operation at the parallel flow field design. The quasi-normalised flow rate corresponds to 0.2 cm³/min·cm² which can be contrasted to 1.4 cm³/min·cm² and 1.8 cm³/min·cm² used in rectangular channel VFBs reported by Chromik et al.[55] and by Charvát et al.,[23] respectively. In those works, capacity utilisations of approximately 85% and 40% were achieved at current densities of 100 mA/cm² and 300 mA/cm², respectively. Meanwhile, Xu et al. reported a VFB with a parallel flow field operating at 0.03 cm³/min·cm², but no capacity data was reported.[56] Indeed, high mass transfer overpotentials quickly activate voltage cut-off values under galvanostatic conditions, aided by the nearly static average velocity of electrolyte within the felt in a parallel flow field (Table 1). Electrolyte velocity at the flow channels is clearly predominant in this design. Naturally, the felt electrode experiences higher fluid velocities near the interphase with the flow channels, but this is not accounted by the average values. In other words, practical capacity utilisation necessitates rectangular channels or interdigitated flow fields, where electrolyte velocities within the graphite felts are greater.[57] Still, to explore if introducing a pulsating flow improves the performance at higher electrolyte flow rates, an additional measurement at a net flow rate of 25 cm³/min with 0.40 cm³ PV and 2.4 Hz PF was performed (see Supporting Information, Figure S9). Under these conditions, the VFB reached a capacity utilisation of 16.0% (1850.5 C), confirming that the strategy applying pulsating flow to typical flow rates should be further studied. It should be noted that the maximum PV of 0.40 cm³ was limited by the metering pump and greater values could be achieved with different equipment.

## Quantification of mass transfer resistance

Electrochemical impedance spectroscopy (EIS) measurements were performed to study the influence of the pulsating electrolyte flow on the mass transfer resistance. The resulting Nyquist plots are depicted on Figure 3(A) whereas the Bode plot can be found in the Supporting Information (Figure S10) along with the fitted parameters (Table S2). Figure 3(B) represents the electrochemical equivalent circuit (EEC) chosen for this electrochemical flow cell, which consists of one parallel R|CPE circuit embedded within a second parallel R|CPE circuit. This EEC can easily fit a wide range of EIS features,[58] including those in

**Table 1.** Parameters describing net flow rates in the VFB fitted with parallel flow fields.

| Net volumetric flow rate [cm³/min] | Average velocity in channels [cm/s] | Average velocity in felt [cm/s] | Quasi-normalised flow rate [cm³/min·cm²] |
|---|---|---|---|
| 5 | 0.232 | 0.0006 | 0.2 |
| 10 | 0.463 | 0.0011 | 0.4 |
| 15 | 0.694 | 0.0017 | 0.6 |
| 20 | 0.926 | 0.0023 | 0.8 |
| 25 | 1.157 | 0.0028 | 1.0 |
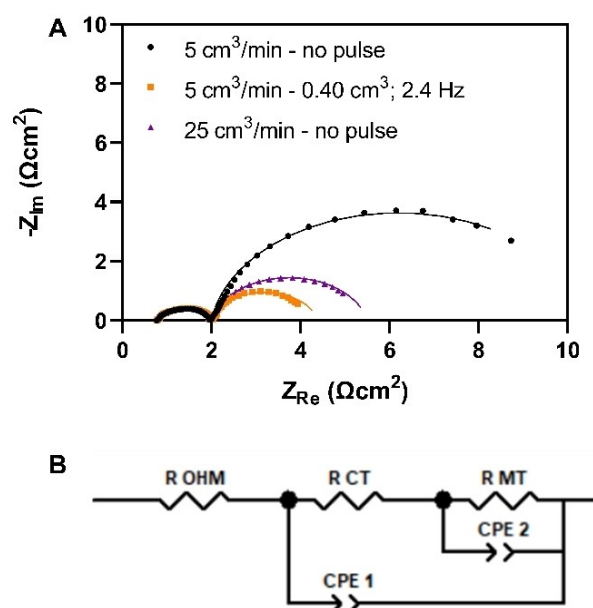


**Figure 3.** A) Nyquist plots for a flow rate of 5 cm³/min without pulsations, a flow rate of 5 cm³/min with pulsations of 0.40 cm³ PV and 2.4 HZ PF and a flowrate of 25 cm³/min without pulsations; B) the electrochemical equivalent circuit.

FBs.[59] In this system, the CPE element in the second R|CPE circuit (CPE 2) takes into account the inhomogeneities of the porous electrodes, and the non-uniform potential and current distribution.[60] A better fit was obtained, since a Warburg element would not be able to capture the EIS response of these non-ideal hydrodynamic porous electrodes.

As seen in Figure 3(A), the second resistance ($R_{CT}$) combines the charge transfer resistance of both electrodes, as confirmed by the depressed arc, which merges two overall time constants.[61] The third resistance ($R_{MT}$) then represents the sum of mass transfer resistances of both half-cells, the lower its magnitude the higher the mass transfer rate. Such physico-chemical interpretation is sufficient to discern between the overall charge transfer and mass transfer resistance and their changes. An EIS analysis of individual half-cells could separate the contribution of each electrode reaction. This was shown by Derr et al., who also demonstrated that the negative half-cell is rate-determining in VFBs.[62] However, such study is outside the scope of this work, requiring a different experimental configuration.[63]

As expected, increasing the electrolyte flow rate from 5 cm³/min to 25 cm³/min without pulsations significantly decreases the overall mass transfer resistance from 8.4 Ω·cm² to 3.5 Ω·cm², respectively. The implementation of a pulsating flow with 0.40 cm³ PV and 2.4 Hz PF for a net flow rate of 5 cm³/min revealed that an overall mass transfer resistance of 2.4 Ω·cm² was achieved in the electrochemical flow cell, which was lower than the mass transfer resistance for both the 5 cm³/min and 25 cm³/min steady flow rate. This proves that the observed effects of a pulsating flow are a result of mass transfer enhancement. Finally, it can be pointed out that the ASR of this

**Batteries & Supercaps**

Research Article
doi.org/10.1002/batt.202300382

**Chemistry Europe**
European Chemical
Societies Publishing

VFB with anion exchange membrane is 0.77 $\Omega \cdot cm^2$, which is similar to other reported laboratory scale VFBs.[23]

## Charge-discharge performance

The VFB was operated for 75 charge-discharge cycles in order to study the influence of the flow regime on its energy storage performance. Four figures of merit were considered as a function of time as the VFB was operated at different electrolyte flow regimes: the efficiencies coulombic efficiency (CE), voltage efficiency (VE) and energy efficiency (EE) and the accessible capacity of the VFB. The efficiencies of the VFB under a constant flow rate of 5 cm³/min and 25 cm³/min without pulsation (Figure 4 part 1, A and B) remained constant during the entire battery cycling at values of 99.0% CE for both flow rates, 70.7% and 67.3% VE and 69.9% and 66.6% EE for 5 cm³/min and 25 cm³/min, respectively. In contrast, the performance of the VFB operated at a constant net flow of 5 cm³/min and a pulsating electrolyte flow (0.40 cm³ PV, 2.4 Hz) displayed initial fluctuations of the CE, VE and EE. However, the efficiencies became stable at 98.4%, 70.5% and 69.4% respectively, showing no further decline over time during of the experiment (Figure 4 part 1, C).

As shown in Figure 4 part 2, the initial accessible discharge capacity increased from 493.2 C in the VFB operating at constant 5 cm³/min to 620.4 C in the one operating at constant 25 cm³/min. Yet, the highest accessible capacity of 701.8 C was achieved under the pulsating electrolyte flow with a constant net flow of 5 cm³/min and 0.40 cm³ PV and 2.4 Hz. In other words, the accessible capacity was the highest under the pulsating flow. As discussed in the case of the cell voltage vs capacity curves, this is again the result of overpotentials in the cell being decreased by higher mass transfer, which in turns delays reaching voltage cut-offs under galvanostatic battery cycling. Clearly, an improved use of accessible capacity requires higher net flow rates.

To determine the effect of flow regime on capacity loss and crossover, the average discharge capacity of the last 5 cycles was compared to the discharge capacity of the first cycle. The battery cycling recorded at a flow rate of 5 cm³/min without pulsations was the shortest due to the short duration of its cycles, resulting in the smallest capacity loss of 6.6% compared to the first cycle. Meanwhile, the measurements with a steady net flow rate of 25 cm³/min and a pulsating flow rate of 2.4 Hz and 0.40 cm³ at 5 cm³/min yielded comparable capacity losses of 11.7% and 10.6%, respectively. This result is noteworthy as the VFB cycling under pulsating flow took 1.4 times longer due to its extended cycle length. Plus, this is consistent with the similar mass transfer rates seen in Figure 3(A) for these two flow regimes.

Comparing Figure 4 part 2, (A) and (C) (no pulsation vs. pulsation at same net flow rates) shows that the pulsating flow with its overall capacity loss of 10.6% appears to imply a larger crossover volume than the flow regime without pulsations with its capacity loss of 6.6%. This might be related to greater convection due to enhanced or asymmetrical pressure at the half-cells. However, the dissimilar cycle duration and the noisy output of the experiment with pulsating flow prevents us from offering a definitive statement on the relationship between pulsating flow and crossover at this point, especially considering that the accessible capacity is influenced by the mass transfer overpotentials in the applied galvanostatic charge-discharge regime. It is acknowledged that pressure monitoring and convection-driven crossover are important features to further study in any FB under pulsating flow by implementing a potential hold step after galvanostatic steps.
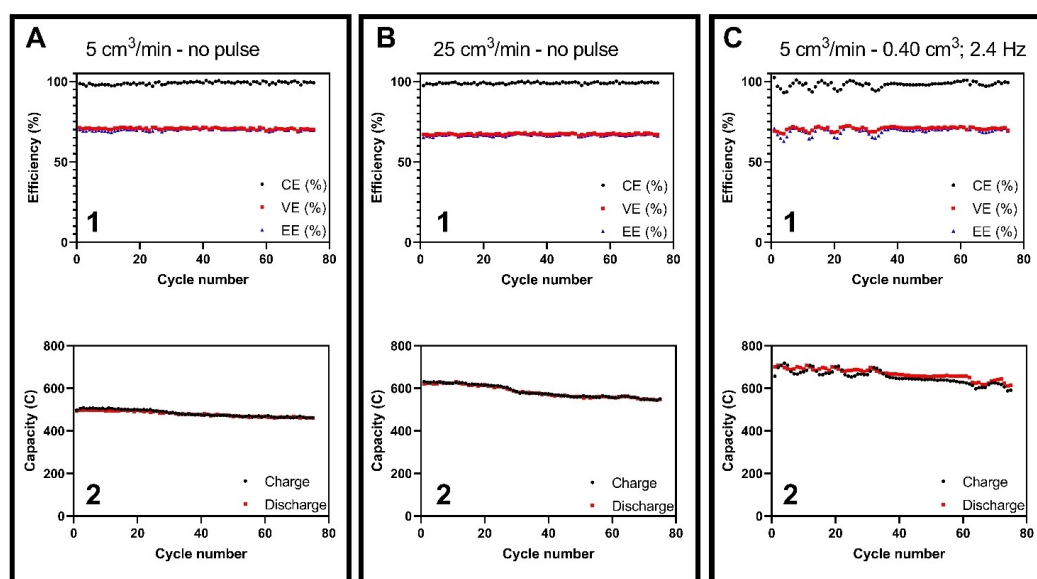


**Figure 4.** Performance of the VFB as indicated by efficiencies (part 1) and accessed capacity (part 2) over 75 cycles for various flow regimes: A) 5 cm³/min without pulsations; B) 25 cm³/min without pulsations; and C) 5 cm³/min pulsating flow with 0.40 cm³ PV and 2.4 Hz PF. Duration of experiments: A) 8.02 h; B) 9.73 h; and C) 13.71 h.
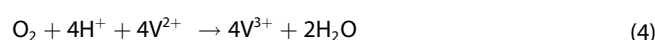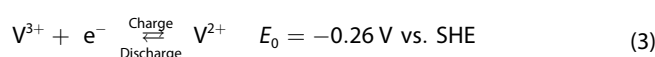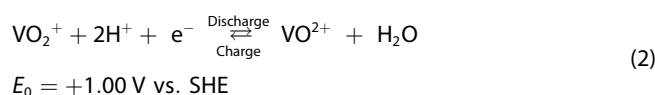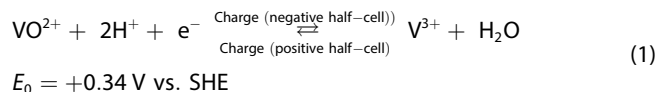
## Conclusions

In this work we investigated for the first time the influence of a pulsating flow regime on the VFB performance, taking both PV and PF into account. If the minimal values of 0.07 cm$^3$ PV and 0.4 Hz PF are surpassed in a flow cell with parallel flow fields, increasing either the PV or the PF while keeping the other parameter and the flow rate constant lead to an enhanced discharge capacity. At the maximum PV and PF values of 0.40 cm$^3$ and 2.4 Hz the discharge accessible capacity was increased by 38.7% compared to the same net 5 cm$^3$/min without pulsations. Additionally, the observed rise in discharge capacity exceeded the performance achieved with a constant steady-state flow of 25 cm$^3$/min, making a fivefold reduction of the net flow rate without performance loss possible. EIS attributes these effects to a reduction of the mass transfer resistance by a factor of 3.5 by the pulsating flow. While significant advantages of a pulsating flow regime have been demonstrated at an overall low flow rate range of 0.2 cm$^3$/min·cm$^2$, future work should evaluate this effect with larger PVs at higher net flow rates for a useful depth of discharge, seeking to implement interdigitated flow fields for faster average electrolyte velocity in the carbon felt.[57] Moreover, an optimisation of current density, wider range of PV, PF and net flow rate is possible to maximise power output and accessible capacity. Attention should be given to the development of models that describe the pulsating flow regime in order to fully understand its influence on the performance of VFBs. It is recognised that mechanical integrity of membranes in stacks under cyclic pressure loads would require a careful design of flow fields,[64] perhaps alongside the use of reinforced membranes.

## Experimental Section

### Substances and materials

A commercial, additive-free VFB electrolyte solution with a total concentration 1.6 M vanadium species and 3.6 M sulfuric acid was obtained from GfE Metalle und Materialien GmbH (Germany). The PAN based Sigracell graphite felt (GFD 4.65 EA IW1) was acquired from SGL Carbon (Germany) and the Fumasep FAP-450 anion exchange membrane from Fuel Cell Store (USA). Solid impervious graphite plates were purchased from Müller & Rössner GmbH & Co. KG (Germany). Grade 5.0 argon gas was supplied by Air Liquide (Belgium).

$$VO^{2+} + 2H^+ + e^- \underset{\text{Charge (positive half-cell)}}{\overset{\text{Charge (negative half-cell))}}{\rightleftarrows}} V^{3+} + H_2O$$

$$E_0 = +0.34 \text{ V vs. SHE} \tag{1}$$

$$VO_2^+ + 2H^+ + e^- \underset{\text{Charge}}{\overset{\text{Discharge}}{\rightleftarrows}} VO^{2+} + H_2O$$

$$E_0 = +1.00 \text{ V vs. SHE} \tag{2}$$

$$V^{3+} + e^- \underset{\text{Discharge}}{\overset{\text{Charge}}{\rightleftarrows}} V^{2+} \quad E_0 = -0.26 \text{ V vs. SHE} \tag{3}$$

$$O_2 + 4H^+ + 4V^{2+} \rightarrow 4V^{3+} + 2H_2O \tag{4}$$

### Cell configuration and flow circuit

The VFB used to perform the electrochemical characterisation was produced in-house using a CNC mill (Euromod MP45, Imes). Figure 5 depicts an exploded view of this electrochemical flow cell consisting of two identical half-cells, which were separated by a Fumasep FAP-450 anion exchange membrane with a dry thickness of 50 micrometres. The use of this membrane significantly reduces vanadium crossover compared to cation exchange membranes.[47] The membrane had an active wet surface of 25 cm$^2$, which was employed to calculate current density. On each side of the cell, the electrolyte tubing went through the aluminium backplate (1), the insulator (2) and the copper current collector (3) before being connected directly to the graphite monopolar plates (4). Parallel flow field channels were milled into compartments which held each of the two graphite felt electrodes (5), both at a compression of 50%. The electrode dimensions were 50 mm×50 mm×4.65 mm with a porosity of 94% before compression.[48] In order to prevent electrolyte leakage, a Viton° gasket (6) was placed between each graphite plate and the membrane (7). The flow cell was sealed mechanically with bolts tightened to 2.5 Nm each.
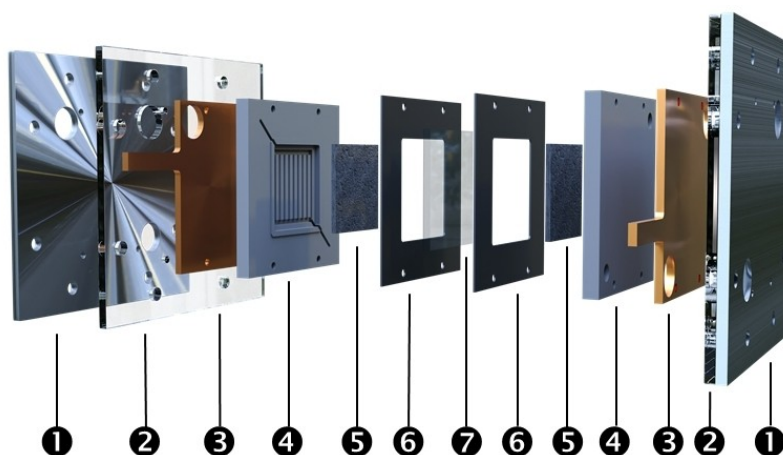


**Figure 5.** Exploded view of the VFB components: aluminium backplates (1), PMMA insulator plates (2), copper current collectors (3), impervious graphite monopolar plates (4) providing parallel flow channels and a compartment for the graphite felt electrodes (5), gaskets (6) and Fumasep FAP-450 membrane (7).

**Batteries & Supercaps**

Research Article
doi.org/10.1002/batt.202300382

**Chemistry Europe**
European Chemical
Societies Publishing

The experimental arrangement is shown schematically in Figure 6. Each of the two reservoirs (2) stored 75 cm$^3$ of vanadium electrolyte, which represents a theoretical capacity of 11,578 C for this volume of electrolyte. In practice, one of the reservoirs limits the battery capacity. Initially, vanadium was present as V(III) and V(IV) species in a 1:1 molar ratio, which corresponds to a state of charge (SoC) of $-50\%$. Consequently, in order to obtain the catholyte (electrolyte containing V(IV) and V(V) for the positive half-cell) and the anolyte (electrolyte containing V(III) and V(II) for the negative half-cell), a pre-charging step was necessary prior to the VFB operation [Equation (1)]. The electrode reactions of the V(IV)/V(V) and V(III)/V(II) redox couples taking place during the operation of the battery are represented by Equations (2) and (3), respectively. Argon gas (1) was employed to purge the electrolytes (2) before the experiments and to remove oxygen from the system. Oxygen spontaneously reacts with V(II), which is a strong reducing agent [Equation (4)], resulting in discharge of the negative electrode and loss of Coulombic efficiency.[49,50] The electrolyte reservoirs were connected through a valve (3), which was closed during the measurements but was opened to mix and rebalance the electrolytes. When necessary, the rebalancing of the electrolyte started by flushing the flow system with argon, then the rebalancing took place under atmospheric pressure while the valve was opened. Lastly the valve was closed, and the system was flushed with argon. A multi-channel peristaltic pump (LabN1, Shenchen) (4) recirculated the electrolytes through the pulsators (5) and electrochemical flow cell (6). The pulsator devices were produced by removing the check valves of two metering pumps (Beta BT4b, ProMinent). All experiments were carried out at a room temperature of $\approx 22 \pm 2\,°C$.

The average linear velocity of the electrolyte at the channels of the parallel flow field and within the porous felt electrodes was estimated using the Equations (5)–(7) proposed by MacDonald and Darling.[51] In these equations $\overline{v_{ch}}$ is the average velocity at the channels, $Q$ the volumetric flow rate, $N$ the number of channels, $A_{ch}$ the cross-sectional area of the channel, $\overline{v_e}$ the average superficial intraelectrode velocity, $k$ the permeability of the electrode, $\psi$ a correction factor which is defined as 1.06 for square channels, $d_h$ the hydraulic diameter, $\varepsilon$ the porosity of the electrode, $d_f$ the fibre diameter and $K_{CK}$ the Carman-Kozeny constant.

$$\overline{v_{ch}} = \frac{Q}{N \cdot A_{ch}} \tag{5}$$

$$\overline{v_e} = \frac{32kQ}{\psi^2 d_h^{\,2} A_{ch}} \tag{6}$$

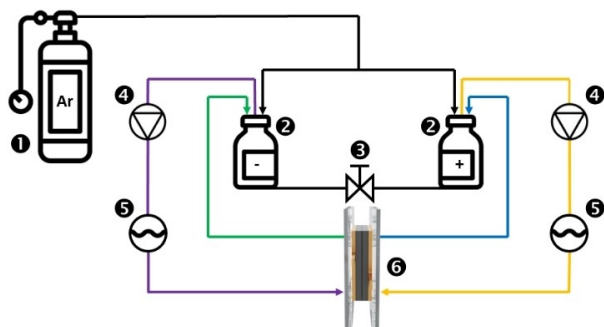$$k = \frac{\varepsilon^3 d_f^{\,2}}{16 K_{CK}(1-\varepsilon)^2} \tag{7}$$



**Figure 6.** Schematic overview of the experimental arrangement.

The permeability was calculated by considering a fibre diameter of $8.18 \pm 0.92$ (SD) micrometres, which was an average of 18 measurements taken with a M165C (Leica) optical microscope for samples of the Sigracell GFD 4.65 EA IW1 (Figures S1–S6). Meanwhile, porosity of the uncompressed felt was corrected for 50% compression by implementing the Equation (8) proposed by Bureš et al.,[52] yielding a value of 88%.

$$\varepsilon = 1 - \frac{1-\varepsilon_0}{1-CR} \tag{8}$$

In that expression $\varepsilon_0$ and $\varepsilon$ represent the porosity of the felt before and after compression, respectively, while the relative compression ratio (CR) is given subtracting the ratio of the compressed felt thickness to the initial thickness from unity.[53] The Carman-Kozeny constant was estimated from the value determined by Charvát et al. for a felt with similar properties: 5.22.[23] The electrolyte velocity is likely somewhat faster at the channels, with more mixing at the boundary with the graphite felt due to the non-ideal insertion of the felt into the channels. Estimated average velocities and a quasi-normalised flow rate are given in Table 1. The quasi-normalised flow rate divides volumetric flow rate by projected active area. While useful to compare different flow fields, it neglects the effect of channel and electrode thickness. The quasi-normalised flow rate of the employed parallel flow fields is relatively low.

### Battery characterisation

#### Voltage vs. capacity curves during discharge

Unless specified otherwise, the measurements were performed using a bi-directional DC power supply (IT-M3412, Itech). Before the start of each experiment, the electrolyte was rebalanced and 25 preparation galvanostatic charge-discharge cycles were performed at a flow rate of 25 cm$^3$/min (1 cm$^3$/min·cm$^2$) without pulsations. A constant current density of $\pm 100$ mA/cm$^2$ ($\pm 2.5$ A) was applied along cut-off cell voltages of 1.65 V and 0.8 V for the charge and discharge step, respectively. These preparation cycles were performed for two reasons, first, to ensure that no residual oxygen was left in the system, second, to create a reference point so that each experiment started at the same battery capacity (635.7 C, within $\pm 2.7\%$) following the successful rebalancing of the electrolytes.

The accessible discharge capacity of the VFB was determined for various flow parameters (Table 2) as taken from voltage vs capacity curves. For each parameter setting four full charge-discharge cycles were first performed at a constant current density of $\pm 100$ mA/cm$^2$ ($\pm 2.5$ A) to ensure a reproducible operation. The battery was then charged to a cut-off value of 1.65 V before recording the discharge capacity of that parameter setting from its respective voltage vs capacity curve. A maximum of five different settings were subsequently recorded. Five charge-discharge cycles at a flow rate of 25 cm$^3$/min were performed after that without pulsations and

**Table 2.** Various parameter settings for the pulsating flow in the VFB at a net flow rate of 5 cm$^3$/min.

| Pulse volume, PV [cm$^3$] | Pulse frequency, PF [Hz] |
|---|---|
| 0.00 | 0.0 |
| 0.04 | 0.6 |
| 0.16 | 1.2 |
| 0.28 | 1.8 |
| 0.40 | 2.4 |

**Batteries & Supercaps**

Research Article
doi.org/10.1002/batt.202300382

**Chemistry Europe**
European Chemical
Societies Publishing

compared to the preparation cycles to confirm that capacity losses during the measurement due to vanadium crossover had no significant influence; capacity loss was no larger than 5.1% from the initial value in all cases. New procedures could be then carried out after rebalancing the electrolyte and performing 25 preparation cycles as mentioned above. Regarding the flow parameters, flow rates of 5, 10, 15, 20 and 25 $cm^3$/min were measured without pulsations. For experiments involving pulsating flow, a constant net flow rate of 5 $cm^3$/min (0.2 $cm^3$/min·$cm^2$) was considered, unless otherwise stated. The PV, corresponding to the pulsed volume displacement, and the PF, corresponding to number of pulses over time, were varied from 0.04 $cm^3$, 0.16 $cm^3$, 0.28 $cm^3$ to 0.40 $cm^3$ and from 0.6 Hz, 1.2 Hz, 1.8 Hz to 2.4 Hz, respectively. All the combinations between these PV and PF values were studied, see Table 2. Capacity utilisation was defined as the ratio between accessed capacity and the theoretical capacity of the battery.

### Electrochemical impedance spectroscopy

Electrochemical impedance spectroscopy was performed using a PGSTAT302 N potentiostat-galvanostat (Metrohm). Each measurement was performed at 100% SoC, which was realised through the following procedure. The battery was first charged at a constant current density of 100 mA/$cm^2$ (2.5 A) until a cut-off voltage of 1.48 V was reached. The battery was then kept under a potentiostatic step at the same voltage. The charge was considered complete when the current reached a value below 10 mA. The employed frequency scan range for the EIS was between 10 kHz to 0.1 mHz. Measurements were taken at 12 points per decade on a logarithmic scale, with a sinusoidal potential amplitude of 10 mV. The analysis tool provided by the Nova (Metrohm) software was utilised to determine the values of the relevant equivalent circuit elements.

### Charge-discharge performance

In order to determine the performance of the VFB operating with a pulsating electrolyte flow, 75 charge-discharge cycles were recorded at a flow rate of 5 $cm^3$/min, a PV of 0.40 $cm^3$ and a PF of 2.4 Hz. These pulsating flow settings were chosen because they were the most effective settings studied in this work. For contrast, the performance of VFBs operating without pulsations was also recorded for 75 charge-discharge cycles at a flow rate of 5 $cm^3$/min and 25 $cm^3$/min. All experiments were preceded by 25 preparation galvanostatic charge-discharge cycles performed in the same manner as for the voltage vs capacity curves. CE was determined for each cycle by dividing the discharge capacity by the charge capacity [(Equation 9)]. The VE was calculated by comparing the average cell voltage measured during discharge operation to the average cell voltage measured during charge operation [Equation (10)]. The EE, which quantifies the amount of energy that can be extracted from a battery relative to the energy input into the system, was given by the product of CE and VE [Equation (11)]. These metrics provide insights into the effectiveness of the battery in terms of its charging and discharging performance. Additionally, the loss in accessible discharge capacity was evaluated to monitor the expected vanadium crossover.

$$CE = \frac{Q_{discharge}}{Q_{charge}} = \frac{\int I_{discharge}(t) \cdot dt}{\int I_{charge}(t) \cdot dt} \tag{9}$$

$$VE = \frac{\int E_{discharge}(t) \cdot dt}{\int E_{charge}(t) \cdot dt} \tag{10}$$

$$EE = CE \cdot VE \tag{11}$$

## Supporting Information

The authors have cited additional references within the Supporting Information.[65]

## Conflict of Interests

The authors declare no conflict of interest.

## Data Availability Statement

The data that support the findings of this study are available from the corresponding author upon reasonable request.

[1] European Environment Agency, "Share of energy consumption from renewable sources in Europe (8th EAP)", can be found under http://www.eea.europa.eu/ims/share-of-energy-consumption-from **2022** (accessed 13 November 2023).
[2] K. Guerra, P. Haro, R. E. Gutiérrez, A. Gómez-Barea, *Appl. Energy* **2022**, *310*, 118561.
[3] A. Mikhaylov, *Energies* **2022**, *15*, 1397.
[4] J. Mitali, S. Dhinakaran, A. A. Mohamad, *Energy Storage Sav.* **2022**, *1*, 166–216.
[5] J. Luo, B. Hu, M. Hu, Y. Zhao, T. L. Liu, *ACS Energy Lett.* **2019**, *4*, 2220–2240.
[6] A. A. Kebede, T. Kalogiannis, J. Van Mierlo, M. Berecibar, *Renewable Sustainable Energy Rev.* **2022**, *159*, 112213.
[7] M. Jafari, A. Botterud, A. Sakti, *Renewable Sustainable Energy Rev.* **2022**, *158*, 112077.
[8] M. M. Rahman, A. O. Oni, E. Gemechu, A. Kumar, *Energy Convers. Manage.* **2020**, *223*, 113295.
[9] H. Zhang, C. Sun, *J. Power Sources* **2021**, *493*, 229445.
[10] J. Kim, H. Park, *J. Power Sources* **2022**, *545*, 231904.
[11] A. R. Dehghani-Sanij, E. Tharumalingam, M. B. Dusseault, R. Fraser, *Renewable Sustainable Energy Rev.* **2019**, *104*, 192–208.
[12] Y. Xu, B. Zhang, *ChemElectroChem* **2019**, *6*, 3214–3226.
[13] D. N. Buckley, A. Bourke, N. Dalton, M. Alhajji Safi, D. Oboroceanu, V. Sasikumar, R. P. Lynch, in *Flow Batteries*, Vol.2 (Eds.: C. Roth, J. Noack, M. Skyllas-Kazacos), Wiley, Weinheim **2023**, pp. 563–587.
[14] A. Parasuraman, T. Mariana, C. Menictas, M. Skyllas-kazacos, *Electrochim. Acta* **2013**, *101*, 27–40.
[15] K. J. Kim, M.-S. Park, Y.-J. Kim, J. H. Kim, S. X. Dou, M. Skyllas-Kazacos, *J. Mater. Chem. A* **2015**, *3*, 16913–16933.

**Batteries & Supercaps**

Research Article
doi.org/10.1002/batt.202300382

**Chemistry Europe**
European Chemical
Societies Publishing

[16] A. Mularczyk, M. Vera, A. Forner-Cuenca, *ChemRxiv.* **2023**, *preprint*, DOI: 10.26434/chemrxiv-2023-2zthc.

[17] A. Bhattarai, N. Wai, R. Schweiss, A. Whitehead, T. M. Lim, H. H. Hng, *J. Power Sources* **2017**, *341*, 83–90.

[18] J. Xu, Y. Zhang, Z. Huang, C. Jia, S. Wang, *Energy Fuels* **2021**, *35*, 8617–8633.

[19] L. F. Arenas, J. J. H. Pijpers, in *Encyclopedia Energy Storage*, Vol. 2 (Ed.: L. F. Cabeza), Elsevier, Oxford **2022**, pp. 524–534.

[20] Q. Wang, Z. G. Qu, Z. Y. Jiang, W. W. Yang, *Appl. Energy* **2018**, *213*, 293–305.

[21] P. C. Ghimire, A. Bhattarai, R. Schweiss, G. G. Scherer, N. Wai, Q. Yan, *Appl. Energy* **2018**, *230*, 974–982.

[22] M. Y. Lu, W. W. Yang, X. S. Bai, Y. M. Deng, Y. L. He, *Electrochim. Acta* **2019**, *319*, 210–226.

[23] J. Charvát, P. Mazúr, J. Dundálek, J. Pocedič, J. Vrána, J. Mrlík, J. Kosek, S. Dinter, *J. Energy Storage* **2020**, *30*, 1014682.

[24] Y. A. Gandomi, D. Aaron, M. M. Mench, in *Flow Batteries*, Vol. 2 (Eds.: C. Roth, J. Noack, M. Skyllas-Kazacos), Wiley, Weinheim **2023**, pp. 607–626.

[25] R. M. Darling, M. L. Perry, *J. Electrochem. Soc.* **2014**, *161*, A1381–A1387.

[26] C. R. Dennison, E. Agar, B. Akuzum, E. C. Kumbur, *J. Electrochem. Soc.* **2016**, *163*, A5163–A5169.

[27] X. Ke, J. M. Prahl, I. J. D. Alexander, J. S. Wainright, T. A. Zawodzinski, R. F. Savinell, *Chem. Soc. Rev.* **2018**, *47*, 8721–8743.

[28] D. S. Aaron, Q. Liu, Z. Tang, G. M. Grim, A. B. Papandrew, A. Turhan, T. A. Zawodzinski, M. M. Mench, *J. Power Sources* **2012**, *206*, 450–453.

[29] Z. N. Duan, Z. G. Qu, Q. Wang, J. J. Wang, *Appl. Energy* **2019**, *250*, 1632–1640.

[30] R. De Wolf, M. De Rop, J. Hereijgers, *ChemElectroChem* **2022**, *9*, e202200640.

[31] A. Forner-Cuenca, E. E. Penn, A. M. Oliveira, F. R. Brushett, *J. Electrochem. Soc.* **2019**, *166*, A2230–A2241.

[32] K. M. Tenny, A. F. Cuenca, Y. M. Chiang, F. R. Brushett, *J. Electrochem. Energy Convers. Storage* **2020**, *17*, 041108.

[33] X. Ni, S. Gao, R. H. Cumming, D. W. Pritchard, *Chem. Eng. Sci.* **1995**, *50*, 2127–2136.

[34] N. Reis, C. N. Gonçalves, M. Aguedo, N. Gomes, J. A. Teixeira, A. A. Vicente, *Biotechnol. Lett.* **2006**, *28*, 485–490.

[35] E. Pérez-Gallent, C. Sánchez-Martínez, L. F. G. Geers, S. Turk, R. Latsuzbaia, E. L. V. Goetheer, *Ind. Eng. Chem. Res.* **2020**, *59*, 5648–5656.

[36] N. G. Carpenter, E. P. L. Roberts, *Inst. Chem. Eng. Symp. Ser.* **1999**, *77*, 309–318.

[37] P. Stonestreet, A. P. Harvey, *Chem. Eng. Res. Des.* **2002**, *80*, 31–44.

[38] A. P. Harvey, M. R. Mackley, P. Stonestreet, *Ind. Eng. Chem. Res.* **2001**, *40*, 5371–5377.

[39] A. P. Harvey, M. R. Mackley, T. Seliger, *J. Chem. Technol. Biotechnol.* **2003**, *78*, 338–341.

[40] M. Vranckaert, H. P. L. Gemoets, R. Dangreau, K. Van Aken, T. Breugelmans, J. Hereijgers, *Electrochim. Acta* **2022**, *436*, 141435.

[41] H. G. Gomaa, A. M. A. Taweel, *Heat Mass Transfer* **2006**, *43*, 371–379.

[42] A. Yahya, S. Hammouda, S. Slimene, H. Dhahri, *Int. J. Therm. Sci.* **2022**, *174*, 107437.

[43] C. Y. Ling, H. Cao, M. L. Chng, M. Han, E. Birgersson, *J. Power Sources* **2015**, *294*, 305–311.

[44] C. R. Brunold, J. C. B. Hunns, M. R. Mackley, J. W. Thompson, *Chem. Eng. Sci.* **1989**, *44*, 1227–1244.

[45] C. Choi, S. Kim, R. Kim, Y. Choi, S. Kim, H. young Jung, J. H. Yang, H. T. Kim, *Renewable Sustainable Energy Rev.* **2017**, *69*, 263–274.

[46] A. H. Whitehead, in *Flow Batteries*, Vol. 1 (Eds.: C. Roth, J. Noack, M. Skyllas-Kazacos), Wiley, Weinheim **2023**, pp. 175–191.

[47] P. C. Ghimire, A. Bhattaraj, N. Wai, T. M. Lim, in *Flow Batteries*, Vol. 2 (Eds.: C. Roth, J. Noack, M. Skyllas-Kazacos), Wiley, Weinheim **2023**, pp. 589–606.

[48] SGL CARBON GmbH, "Sigracell® Battery Felts", can be found under http://www.sglcarbon.com/en/markets-solutions/material/sigracell-battery-felts **2021** (accessed 13 November 2023).

[49] K. Ngamsai, A. Arpornwichanop, *Energy Procedia* **2014**, *61*, 1642–1645.

[50] K. Lourenssen, J. Williams, F. Ahmadpour, R. Clemmer, S. Tasnim, *J. Energy Storage* **2019**, *25*, 100844.

[51] M. MacDonald, R. M. Darling, *AIChE J.* **2018**, *64*, 3746–3755.

[52] M. Bureš, Z. Tomiška, J. Charvát, M. Svoboda, P. Richtr, J. Pocedič, J. Kosek, P. Mazúr, A. Zubov, *Chem. Eng. J.* **2023**, *458*, 141424.

[53] C. L. Hsieh, P. H. Tsai, N. Y. Hsu, Y. S. Chen, *Energies* **2019**, *12*, 313.

[54] D. Aaron, Z. Tang, A. B. Papandrew, T. A. Zawodzinski, *J. Appl. Electrochem.* **2011**, *41*, 1175–1182.

[55] A. Chromik, A. R. dos Santos, T. Turek, U. Kunz, T. Häring, J. Kerres, *J. Membr. Sci.* **2015**, *476*, 148–155.

[56] Q. Xu, T. S. Zhao, P. K. Leung, *Appl. Energy* **2013**, *105*, 47–56.

[57] Z. Huang, A. Mu, L. Wu, H. Wang, *J. Energy Storage* **2022**, *45*, 103526.

[58] A. R. C. Bredar, A. L. Chown, A. R. Burton, B. H. Farnum, *ACS Appl. Energ. Mater.* **2020**, *3*, 66–98.

[59] V. Muñoz-Perales, M. van der Heijden, P. A. García-Salaberri, M. Vera, A. Forner-Cuenca, *ACS Sustainable Chem. Eng.* **2023**, *11*, 12243–12255.

[60] J. B. Jorcin, M. E. Orazem, N. Pébère, B. Tribollet, *Electrochim. Acta* **2006**, *51*, 1473–1479.

[61] N. Meddings, M. Heinrich, F. Overney, J. S. Lee, V. Ruiz, E. Napolitano, S. Seitz, G. Hinds, R. Raccichini, M. Gaberšček, J. Park, *J. Power Sources* **2020**, *480*, 228742.

[62] I. Derr, M. Bruns, J. Langner, A. Fetyan, J. Melke, C. Roth, *J. Power Sources* **2016**, *325*, 351–359.

[63] I. Derr, D. Przyrembel, J. Schweer, A. Fetyan, J. Langner, J. Melke, M. Weinelt, C. Roth, *Electrochim. Acta* **2017**, *246*, 783–793.

[64] R. Gundlapalli, S. Jayanti, *J. Energy Storage* **2021**, *33*, 102078.

[65] L. Eifert, R. Banerjee, Z. Jusys, R. Zeis, *J. Electrochem. Soc.* **2018**, *165*, A2577–A2586.